Walter, T. R., Legrand, D., Delgado Granados, H., Reyes, G., Arámbula, R. (2013): Volcanic eruption monitoring by thermal image correlation: Pixel offsets show episodic dome growth of the Colima volcano. - Journal of Geophysical Research, 118, 4, 1408-1419

DOI: 10.1002/jgrb.50066

JOURNAL OF GEOPHYSICAL RESEARCH: SOLID EARTH, VOL. 118, 1408–1419, doi:10.1002/jgrb.50066, 2013

Volcanic eruption monitoring by thermal image correlation: Pixel offsets show episodic dome growth of the Colima volcano

Thomas R. Walter,[1] Denis Legrand,[2] Hugo Delgado Granados,[2] Gabriel Reyes,[3] and Raúl Arámbula[3]

Received 14 December 2012; revised 18 December 2012; accepted 20 December 2012; published 30 April 2013.

[1] Estimating the magnitude of dome eruptions is one of the main challenges in volcano monitoring. Although modern monitoring networks are in place at many dome-building volcanoes, the type and occurrence of explosive activity and the scale of the eruptions are commonly estimated by visual inspection. Quantifying the deformation of dome-building volcanoes and the occurrence of explosions is highly valuable, not only for enabling the provision of early warnings but also for facilitating an understanding of the physics of explosive volcanoes, as demonstrated by this study of one of the most active volcanoes in Mexico. The Volcán de Colima is currently experiencing a phase of viscous dome growth, which is associated with episodic "Vulcanian" eruptions and rock falls. Little is known about the dynamics of this dome, its growth rates, or the scale of the associated explosions. We present the results from an analysis of nighttime time-lapse infrared images and compare these data with local seismic amplitude recordings. By digital image correlation, we track temperature features in infrared images. Images taken before and after the explosions reveal the location of the hot dome to be subject to significant and systematic lateral pixel offsets. Dome deformation is shown to occur intermittently every 3–4 h, with lateral displacements exceeding 0.3 m within periods of less than 120 s. Only the thermally elevated regions of the western dome, which may represent a coulée-like flow, are displaced. This movement is often, but not always, associated with seismic amplitude peaks. Therefore, our analysis of the infrared image correlation suggests the occurrence of aseismic dome-deformation episodes, thereby challenging the current understanding of dome growth and/or the appropriateness of commonly used volcano surveillance techniques.

Citation: Walter, T. R., D. Legrand, H. D. Granados, G. Reyes, and R. Arámbula (2013), Volcanic eruption monitoring by thermal image correlation: Pixel offsets show episodic dome growth of the Colima volcano, *J. Geophys. Res. Solid Earth*, *118*, 1408–1419, doi:10.1002/jgrb.50066.

1. Introduction

[2] The growth and collapse of volcanoes are most dynamic at dome-building volcanoes, such as the Shiveluch volcano in Kamchatka [*Belousov et al.*, 1999], Mount St. Helens in the U.S. [*Christiansen and Peterson*, 1981], Montserrat in the West Indies [*Hooper and Mattioli*, 2001], Merapi in Indonesia [*Hort et al.*, 2006], Colima in Mexico [*Saucedo et al.*, 2010], and others [*Donnadieu*, 2000; *Voight and Elsworth*, 2000]. Lava domes are massive and volatile-poor extrusion complexes of highly viscous magma, often emplaced in a volcano summit crater region. If such domes overflow the crater rim or otherwise experience a change in slope, they may change into flow-like structures. These coulées may continue flowing downslope for hundreds of meters [*Fink and Anderson*, 2000]. Lava domes may extrude over the course of years or even decades. However, significant fluctuations over short time scales (seconds or minutes) are likely to be common [*Johnson et al.*, 2008]. Lava domes that are subject to growth may intermittently destabilize, producing rock falls and pyroclastic flows [*Voight*, 2000]. As these dome collapses are often initiated on the flanks of a lava dome, close observations of the growth and spread of the lava dome flanks are crucial for the understanding of associated volcanic hazards.

[3] Dome growth and collapse are thought to be directly related, although it is difficult to quantify dome growth preceding a collapse due to hazardous conditions, restricted field accessibility and other limitations. Consequently, eyewitness accounts are the most important source of information available for many historic eruptions [*Saucedo et al.*, 2010]; in only a few cases,

Additional supporting information may be found in the online version of this article.

[1]Department of Earth Physics, GFZ German Research Center for Geosciences, Telegrafenberg, Potsdam, Germany.
[2]Instituto de Geofísica, UNAM, Mexico City, México.
[3]Observatorio Vulcanológico de la Universidad de Colima, Colima, Mexico.

Corresponding author: T. R. Walter, Department of Earth Physics, GFZ German Research Center for Geosciences, Telegrafenberg, 14473 Potsdam, Germany. (twalter@gfz-potsdam.de)

2169-9313/13/10.1002/jgrb.50066

multiple analog photographs and video recordings taken from approximately the same position have enabled the monitoring of deforming domes [*Yamashina et al*., 1999]. In the present study, we explored the use of a camera in combination with digital image correlation routines and applied the technique to the growing dome of the Volcán de Colima to quantify dome growth. When combined with seismic records, the results obtained in this study imply that dome growth is often but not always associated with detectable seismicity.

1.1. The Colima Dome

[4] The Volcán de Colima (Figure 1) is the most active volcano in Mexico and is situated in close proximity to the cities of Colima (30 km) and Guadalajara (120 km). The viscous dome of the Volcán de Colima has been extruding at the summit for approximately 5 years, and the current consensus is that the area surrounding the volcano should be prepared for another large explosive eruption associated with dome destruction. Situated in the trans-Mexican volcanic belt, Colima's magmatism is linked to the convergence of the Cocos and Rivera plates under the North American plate [*Luhr et al*., 2006]. Over 50 eruptions of the Volcán de Colima have been documented in written records [*Luhr and Carmichael*, 1980], the largest of which occur at the end of lava production cycles [*Luhr*, 2002]. The last major eruption culminated in 1913 and caused pyroclastic deposits as thick as 15 cm at a distance of ~26 km [*Saucedo et al*., 2010], which are associated with lahars [*Davila et al*., 2007], and ashes that traveled as far as ~720 km to the NNE of the vent. More recent eruptive episodes occurred in 1975–1976, 1981–1982, 1991–1994, 1998–1999, 2001–2003, and 2004–2005 [*Jimenez-Escalona et al*., 2011]. The current dome-building phase began in 2007 and has continued since then (until mid-2011), creating a high possibility of a strong explosive eruption (VEI > 4) in the coming years [*Mendoza-Rosas and de la Cruz-Reyna*, 2008]. After a period of quiescence in 2012, dome growth revived again in early 2013.

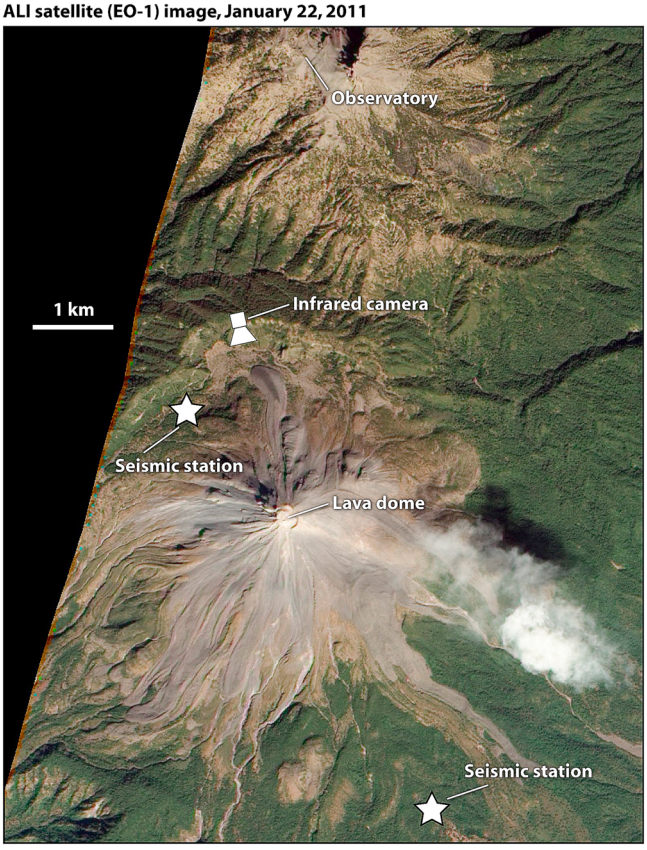

Figure 1. Satellite image of the Volcán de Colima and the location of the camera and the seismic stations investigated in this work.

[5] Although the Volcán de Colima is one of the best monitored volcanoes worldwide, classic geodetic techniques aim at monitoring mainly the mid-to-lower volcano flanks [*Ramirez-Ruiz et al*., 2002]. Knowledge of the modalities of the growing dome within the summit region is commonly derived indirectly using techniques such as video monitoring [Bretón González, personal communication, 2012] and infrared surveys [*Stevenson and Varley*, 2008]. Since 2007, direct and standard geodetic measurements of the growing dome (Figure 2) from GPS and EDM records have been achieved, but these remain difficult to obtain because of the frequent explosions, deployment failure or obscuration, and the generally hazardous access to the top of the volcano. Moreover, remote-sensing methods, such as InSAR and related time-series methods, have so far had limited success in obtaining measurements of the steep and constantly changing volcano surface [*Pinel et al*., 2011]. Therefore, detailed direct measurements of the dome growth have been limited. Consequently, the relationship between dome growth dynamics and seismic activity has not yet been investigated in detail.

1.2. Volcano Camera Monitoring

[6] Recent studies have made increasing use of photographic methods in geological mapping and classification, and these can be broadly categorized into satellite-, aerial- and terrestrial-based methods. The processing of the data obtained using these methods may provide a variety of information, e.g., the distance of an object from the camera and the elevation of the ground. One such application for a specific volcanic hazard has been the topographic mapping of Mount St. Helens during dome growth and the runoff pattern of lahars, which has been thoroughly reviewed [*Dzurisin*, 2007]. Terrestrial photography is gaining in importance, especially as digital video camera systems, which offer continuous footage at reasonable costs, have become available [*Walter*, 2011a; *Diefenbach et al*., 2012]. Video records of volcanoes were still mainly recorded in analog during the 1990s, and analytical methods were conducted manually [*Formenti et al*., 2003]; since then, the use of the digital format has allowed for more advanced tracking methods [*Major et al*., 2008], which often rely on mathematical correlation techniques [*James et al.*, 2009; *Johnson et al.*, 2008]. Most volcano observatories start to deploy webcams in an attempt to continuously record the activity of volcanoes [*Patrick et al*., 2010] and retrieve first-order quantitative parameters, such as the height of eruption plumes, wind shear, and ash dispersion directions and reflectivity changes. Quantitative image analysis and digital flow field computations have significantly contributed to a better understanding of volcano crater deformation, lava lake activity [*Patrick et al*., 2010], lava flow flux variations [*James et al*., 2007; *James et al*., 2012], the extrusion [*Major et al.*, 2009] and collapse of spines [*Walter et al.*, 2011b], the cyclic rise and fall of the lava surface within a lava lake

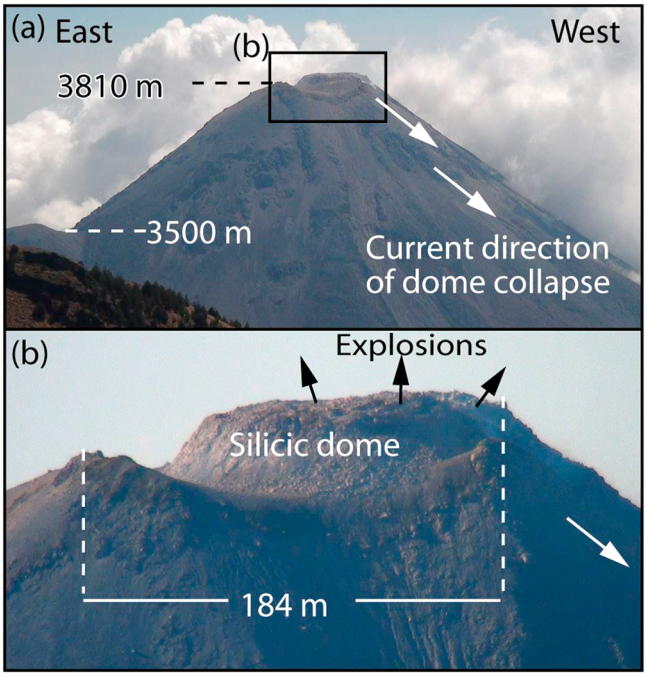

Figure 2. (a) Summit region of the Volcán de Colima as observed from the volcano observatory, which is located 7 km to the north. (b) A viscous dome has grown in recent years, which has almost filled the crater of the Volcán de Colima. The volcano flanks are episodically over-steepening toward failure in the form of rock falls and block-and-ash pyroclastic flows. The failure direction is mainly toward the west (N260°) as indicated by the white arrows in the figure. Also shown are the approximate locations and directions of explosions (black arrows).

[*Orr and Rea*, 2012], and the tracking and monitoring of eruption clouds [*Petersen et al*., 2011].

[7] Although our work focuses on the Colima volcano, earlier studies elsewhere have already demonstrated the relevance and success of the techniques used here. One study utilizing pixel-offset calculations to study volcano dome growth was conducted on the Santiaguito volcano in Guatemala [*Johnson et al*., 2008]. The two volcanoes share many similarities; both are of the dome-building type and have been intensely studied using ground- and satellite-based sensors. Of technical and logistical relevance, both volcanoes are neighbored by a morphologic peak higher than the actual active volcanic center, which makes the testing and application of ground-based imaging methods highly effective. Similar to the Colima volcano, the dome of Santiaguito grows episodically and can be effectively monitored by cameras from the adjacent edifice. Using a particle image velocimetry algorithm, it was shown that eruptions of the Santiaguito volcano are associated with a systematic uplift of the dome on the order of tens of centimeters [*Johnson et al*., 2008]. Dome growth has been shown to be associated with ash-loaded eruptions and accompanied by long-period earthquakes.

[8] In a few cases, camera monitoring is complemented by repeated or even continuous infrared camera measurements that, in addition to being ideal for thermal mapping, have a clear advantage in being effective at night. Infrared imagery has been shown to provide very important information about volcanoes at times of unrest [*Spampinato et al*., 2011], such as during dome-building [*Schneider et al*., 2008] and fumarole activity [*Stevenson and Varley*, 2008]. For a general review of volcanologic applications [*Ramsey and Harris*, 2012] and similar infrared camera types to those used in our study, we refer to the recent literature [*Spampinato et al*., 2011].

[9] Based on 2-D digital image correlation calculations applied to infrared imagery, we aim to detect and quantify the deformation of the Volcán de Colima dome and examine how the results are related to seismic activity. First, we describe the method, which aims to pair and correlate time-lapse images. The data used to investigate dome deformation at Volcán de Colima were obtained using a portable infrared camera. The results section presents a representative example from February 2011, when the dome growth occurred sporadically during explosive events. The digital flow field was quantified and validated against seismic data, and the two data streams showed close agreement. Our results highlight the use of thermal image correlation techniques for the assessment of current activity at Volcán de Colima and other applications such as continuous volcano monitoring programs.

2. Methods

2.1. Data Collection

[10] The field campaign was performed in February 2011, and the data were retrieved from camera records and the permanent local seismic network operated by Colima University (RESCO network).

2.1.1. Camera Records

[11] We used optical, high-definition SLR-video cameras and infrared time-lapse records that were acquired using a forward-looking infrared camera (FLIR P620), which was focused on the summit region of Volcán de Colima (Figure 3). The operation of the standard camera was affected during the day by convective clouds, which obscured the view of the volcano most of the time. However, clear views and less obscuration were obtained by the infrared camera at night, as found in other infrared studies [*Spampinato et al*., 2011]. The FLIR camera, which operates in the 7.5–13 μm wave band, was set to a temperature range of 0–500°C. We selected this range of brightness temperatures because it was assumed that it would cover the expected temperature field associated with the growing dome of Volcán de Colima. The sampling interval was fixed at 1 min (a time-lapse video can be found in the supporting information).

[12] The resolution of the FLIR camera used in this study was 640 × 480 pixels. We combined the camera with a 7° (f = 131) zoom lens with a 0.38 mrad instantaneous field of view. The camera was placed on a solid tripod at a distance of 2590 m north of the dome (N19.53°, W103.62°) as shown in Figure 1. By assuming the 184 m wide crater rim as a reference (Figure 2b), the field of view was translated through geometric transformations to a metric field of view of 238 m × 317 m at the volcanic center, and the infrared pixel dimensions were approximately 1 m × 1 m at the center of the dome (Figures 3 and 4). The viewing direction was SSE, and the field of view contained both the crater and the silicic dome of the Volcán de Colima. We assumed a constant pixel size, although areas represented by pixels closer to the camera

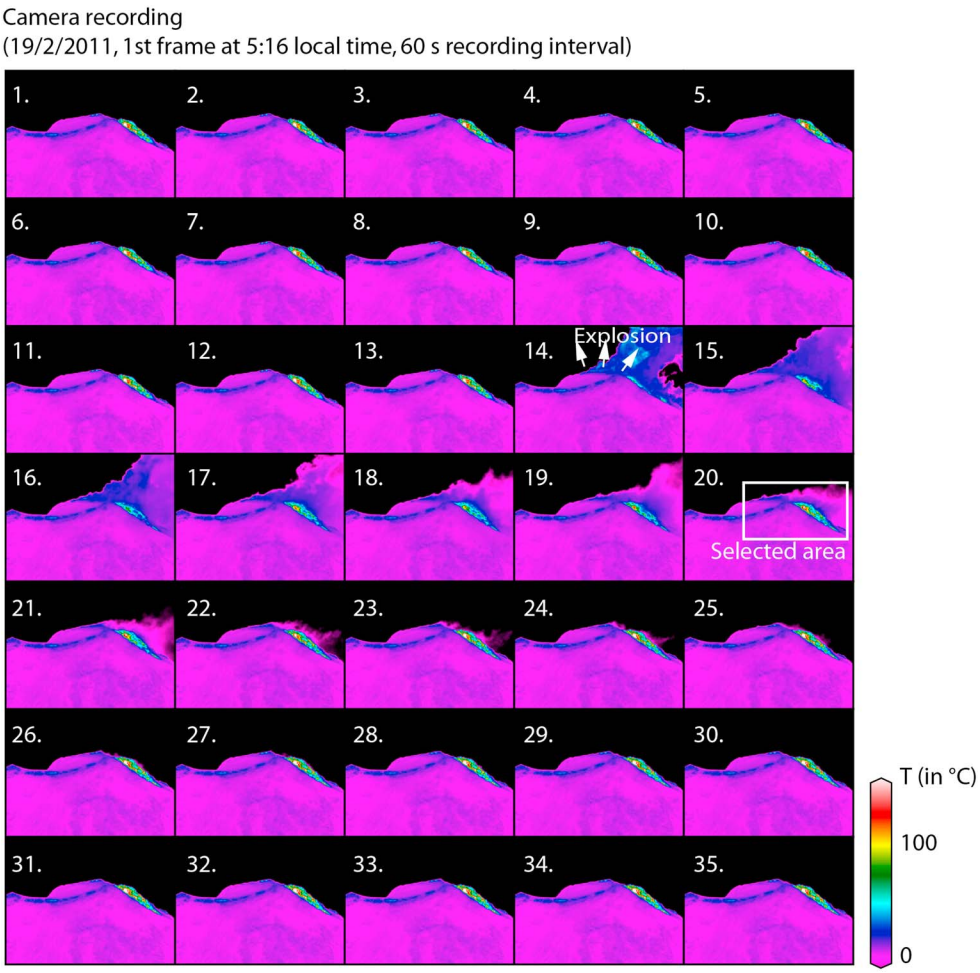

Figure 3. Thermal images of the summit region taken at night from a location north of the Volcán de Colima, 2.59 km from the northern rim of the summit crater. A subset of infrared time-lapse recordings enabled the retrieval of pixels with ~1 m^2 dimensions. This work employed digital image correlation methods to analyze systematic pixel offsets. The white box in frame 20 outlines the area shown in Figure 4. The thermal images shown here are saturated for visualization purposes only. Also shown is the approximate location and direction of explosions (the arrows in frame 14).

at the northern flank of the summit are certainly smaller. As most of the activity, rock falls, and dome growth were expected to be directed toward the west, which is parallel to the field of view, we assumed that the 1 m^2 pixel dimension was a reasonable simplification of the geometric problem.

[13] Thermal data are dependent on a variety of measured object properties and the environment. Temperatures derived from infrared imaging depend mainly on the emissivity of the object, the distance, and travel path to the camera sensor, solar reflection, viewing angle, and the presence of particles/gases in the electromagnetic radiation path [*Spampinato et al.*, 2011, and references therein]. Corrections of unwanted contributions are difficult to achieve yet may largely affect the results [*Ball and Pinkerton*, 2006]. In the present study, we used information from previous studies on the Volcán de Colima [*Stevenson and Varley*, 2008] and assumed a constant emissivity of 0.95. Other environmental effects that may influence the derived temperature, such as meteorological changes and transmissivity, may vary from 0.6–0.8 and depend on humidity [*Stevenson and Varley*, 2008]. We corrected the atmospheric attenuation considering reflected temperature, transmission, and external optics using the FLIR-ThermaCAM Researcher Professional processing software and an emissivity of 0.95, a transmissivity of 0.7, an environmental and path temperature of 10°C, and a humidity of 50%. Obtaining a more accurate atmospheric correction at the steep-sided volcano remained difficult because of the significant elevation distance and associated temporal and spatial variations. As in situ monitoring of the air temperature and humidity at the dome was not feasible because of the danger of explosion, we relied on data recorded by a handheld Kestrel weather station located at the camera site. Remaining atmospheric contributions may be significant [*Ball and Pinkerton*, 2006]; however, associated error contributions do not limit the findings of our study because the emphasis of the study was on the position and pattern of the apparent brightness temperature pattern rather than its temperature values. Moreover, using a normalized image-correlation processing technique, time-dependent temperature variations are largely excluded, as seen by the absence of a diurnal signal in the image-matching analysis results. We aimed to detect and quantify any spatial perturbations

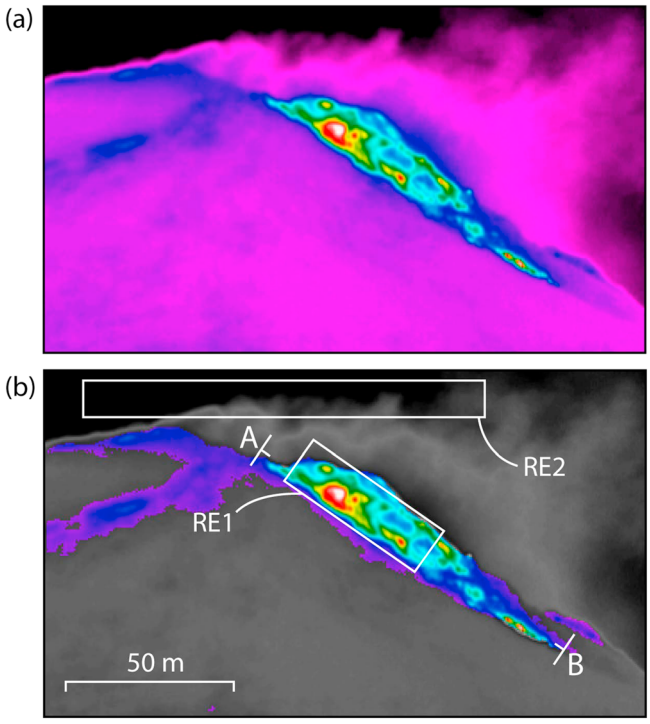

Figure 4. Data selection procedure: (a) illustrated for frame 20 (Figure 3) and (b) after masking out all pixels below an apparent temperature value of 5°C (shown in grayscale). This processing mainly reduces the effect of the insulation during morning and evening hours. The colored regions correspond to selected pixels at temperatures greater than 5°C. Region RE1 was used to compute the mean displacement rate of the dome. Region RE2 was used to detect thermal exhalations. Line A-B indicates the location of the cross section illustrated in Figure 6.

of the intensity matrix in the images, as described further below.

2.1.2. Seismic Recordings

[14] Data from the permanent broadband (Guralp CMG 40TD) seismic station EZV5, located approximately 4 km SSE from the summit (Figure 1), were used as an independent data set; this data set included the timing and, allegedly, the scale of the volcanic explosions. The results obtained from another station are described in the supporting information (Figure S3). In this study, we exploited the seismic positive amplitude (RSAM) of the vertical component. The RSAM summarizes the average positive amplitudes of the ground shake from either earthquakes or volcanic tremor and are herein averaged over intervals of 1 s or longer (see supporting information). We used the RSAM because it is commonly used as a simple but effective way to illustrate seismic activity during periods of volcanic unrest [*Endo and Murray*, 1991]. The RSAM provided a robust measure that is applied by volcano observatories worldwide, which we used in this study to test and validate the activity recorded by the camera.

2.2. Data Analysis

[15] At night, the clear sky made the use of infrared images highly effective, and insulation artifacts were negligible. Spatiotemporal analysis of pixels from the infrared camera data is a flexible and robust method that yields a quantitative description of both the pixel-offset patterns and the thermal exhalation activity.

[16] We used a digital image correlation (DIC) technique, an image-matching method that is common in computer vision studies to extract shape, deformation, and motion measurements [*Sutton et al.*, 2009]. Digital photogrammetry is a relatively new sub-discipline of photogrammetry that was first used in the 1980s [*Konecny*, 1985]. Some of the earliest image-correlation studies were conducted before the invention of digital photography in the 1950s by Hobrough and colleagues to measure changing ground conditions [*Anonymous*, 2003]. After the concepts of digital image acquisition and computer-based deformation measurements in material systems were proposed [*Peters and Ranson*, 1982], the basic concept of comparing smaller sub-regions of an image became common [*Sutton et al.*, 1983]. Shortly thereafter, concepts developed for solid mechanics were applied also to measure the velocity of a fluid system [*Peters et al.*, 1984]. DIC, with its focus on solid systems, and particle image velocimetry (PIV), with its focus on fluid systems, have been applied to many laboratory experiments and terrestrial photogrammetric problems [*Sutton et al.*, 2009]. The field of DIC has grown immensely, especially since 2000, leading to more than 400 articles [*Sutton et al.*, 2009], many of which are related to improving mathematical concepts and accuracy. Image reconstruction improves the accuracy of the matching process (e.g., using higher-order spline functions), thereby reducing measurement bias and resulting in position accuracies of 1/100 of pixel size or better [*Schreier et al.*, 2000]. Further improvements to the search, registration, and correlation procedure as well as the extended method have been thoroughly reviewed [*Sutton et al.*, 2009].

[17] The goal of DIC at the Colima volcano was to detect the same physical points (pixels) recorded in multiple time-lapse images in the infrared spectrum. As a pixel may be defined by a gray value that is similar to that at many other points in the image, the corresponding points can be correctly identified if small neighborhoods around the pixel of interest are considered.

[18] Hereafter, we refer to the first image as the reference image and the second image as the deformed image. We used the DIC technique to investigate time-dependent changes in observables, as shown by local displacements and strains over various temporal and spatial scales. The technique considers the mathematical cross correlation of a digital dataset comprising a two-dimensional array of the intensity values [*Pan et al.*, 2009].

[19] Ideally, the reference image and the deformed image are both acquired with exactly the same optical parameters, i.e., the same camera lens and objective, viewing geometry, and illumination. As we used infrared rather than optical imagery, the intensity values can change due to the apparent changes in brightness temperature and atmosphere, energy emission artifacts, or other shifts in the location of the pixels.

[20] If the intensity values in a given correlation window change with time [*Clocksin et al.*, 2002], e.g., due to insulation effects, then a correlation term may lead to higher correlation values in the brighter parts or may become quantitatively biased by changes in the image amplitude. This limitation was assumed to not be critical because (a) we used a normalization approach, (b) we analyzed the

pattern of the temperature rather than the amplitude, and (c) we compared systematic pixel shifts against an independent data set derived from seismic records.

[21] The basic requirement of the DIC algorithm used here is that the method should be insensitive to variations in the intensity while being sensitive to the offset of intensity variations. Therefore, the following equation was formulated [*Pan et al.*, 2009]:

$$af(x_i, y_j) = g\left(x_i^{'}, y_j^{'}\right); \; i = 1, 2, \ldots, n \tag{1}$$

where the scale factor a affects the intensity change, i refers to the ith pixel, f denotes the grayscale intensity (or temperature) value at a given point with x and y coordinates, and g denotes the shifted pixel pattern in the deformed image.

[22] To estimate the degree of similarity between the reference image and the deformed image, we defined a correlation criterion. Of the variety of definitions reported in the literature [*Pan et al.*, 2009], we chose to use the so-called zero-normalized sum of the squared differences (ZNSSD) method:

$$C_{\mathrm{ZNSSD}} = \sum_{i=-n}^{n} \sum_{j=-n}^{n} \left(\frac{f(x_i, y_j) - f_m}{\Delta f} - \frac{g\left(x_i^{'}, y_j^{'}\right) - g_m}{\Delta g} \right)^2 \tag{2}$$

where

$$f_m = \frac{1}{(2n+1)^2} \sum_{i=-n}^{n} \sum_{j=-n}^{n} f(x_i, y_j), \tag{3}$$

$$g_m = \frac{1}{(2n+1)^2} \sum_{i=-n}^{n} \sum_{j=-n}^{n} g\left(x_i^{'}, y_j^{'}\right) \tag{4}$$

and

$$\Delta f = \sqrt{\sum_{i=-n}^{n} \sum_{j=-n}^{n} \left[f(x_i, y_j) - f_m \right]^2} \tag{5}$$

$$\Delta g = \sqrt{\sum_{i=-n}^{n} \sum_{j=-n}^{n} \left[g\left(x_i^{'}, y_j^{'}\right) - g_m \right]^2}. \tag{6}$$

[23] Rather than tracking individual pixels, we defined squared subsets of $(2n+1) \times (2n+1)$ pixels. These subsets could be more uniquely characterized because each contained a pattern of diverse values that could be easily distinguished from those of other subsets. We aimed to achieve a sub-pixel level of accuracy, which required considering both the subset displacement mapping function and the intensity change [*Pan et al.*, 2009]. The subsets were selected in such a way that they were large enough to contain a distinctive intensity pattern but small enough to achieve a sub-pixel level of accuracy. De-correlation was defined to occur if less than three similar intensity peaks could be identified in a subset. Offsets on the order of 0.05 pixels could be detected, representing a deformation of 5 cm.

[24] The ZNSS method has been proven to be one of the most robust correlation methods [*Pan et al.*, 2009] because it is sensitive to sub-pixel displacements but not to image-wide changes in illumination. Therefore, in the present study, the ZNSSD-method allowed for the exploration of temperature field offsets and had the advantage of being able to discount unwanted effects of environmental artifacts from the results as long as the general pattern was recognizable in the correlated image. Because image intensity patterns are likely to change over the course of hours, we used two strategies. First, we tested our concept on a smaller dataset. We then defined the first image as the reference image and correlated each subsequent image with it. Second, we defined the reference image to be correlated with the image found five frames later. The basic principle of this is the same as that of the first strategy; however, it presents an advantage in that the moving reference image leads to more stable results over longer periods. We quantify pixel offset, although we use the terminology of *deformation* (see section 4). The accurate timing of the short-term deformation episodes and the occurrence of very slow deformations that were below the detection threshold in a five-frame interval may not have been properly represented.

[25] The results are displayed in an image vector format for the selected area. The mean displacement values for the dome were calculated in the region RE1, to which the occurrence of thermal exhalations [see also *Stevenson and Varley*, 2008] in the region RE2 was compared (Figure 4). These results were compared with seismic amplitude records in a time series that covered several distinctive explosion events.

3. Results

[26] In general, the thermal field reflects elevated temperatures at the summit crater rim [*Stevenson and Varley*, 2008]. Additionally, it is worth noting that the identification of a higher-thermal field did not convey the bulk of the morphological features of the expressed dome, which has been growing since 2007. Specifically, most of the dome surface presented no thermal anomalies in our data. Only on the right side of the field of view did a tongue of the dome exhibit elevated temperatures (Figure 3).

[27] During the time-lapse observation periods, a number of explosions were detected at a frequency of approximately 1 event every 3 to 4 h. An example of a nighttime infrared time-lapse dataset is shown in Figure 3. The recording example covers one of the explosions, which is visually associated with an apparent temperature increase above the dome in the eruptive plume. The visual changes were primarily related to the eruption cloud itself; neither the hot part of the dome nor the other regions of the thermally expressed crater rim indicated significant changes in the infrared amplitude or pattern.

[28] Figure 4 shows a subset of the infrared images (frame 20 of Figure 3). Figure 5 shows the results of the DIC in the same image view, and Figure 6 shows the DIC results that focus on specific sub-regions (RE1 and RE2; Figure 4). As seen from the figures, most of the dome appears stable. The crater region of Volcán de Colima and the main crater-filling dome did not exhibit any significant displacement. However, pronounced pixel offsets were observed on the right side of the field of view, which corresponds to the western flank of the dome. We note that the systematic

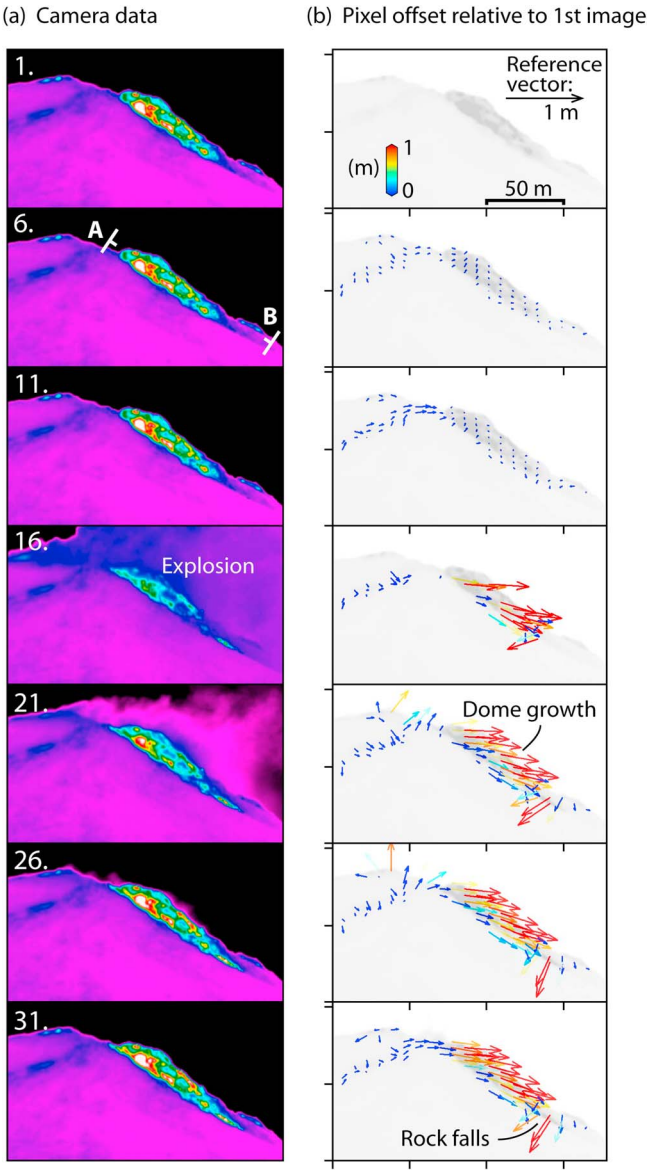

Figure 5. (a) Infrared images and (b) digital cross-correlation results. The first image is the reference image, which was cross-correlated against each subsequent image. For visualization purposes, we show every fifth sample image only. Frame 16 shows some de-correlation effects due to profound steam releases that hindered our observations. The frames recorded after the explosion show a systematic displacement of the thermally elevated region on the right side (the west flank) of the dome. Each frame recorded after the explosion shows a similar pixel offset compared with frame 1. The camera was stable during the recording, as indicated by the stable reference and the stable pixels located elsewhere on the crater rim.

displacements observed on the western flank occurred during the explosive event. The region affected by the deformation corresponds to the region of elevated temperature of the dome. The deformation value exceeded 0.3 m within 120 s (21 m/h). The total displacements (Figure 5, the vectors are shown as |Vx+Vy|) were reasonably uniform over the hot area. At the lowermost front of the deforming volcanic dome, the vector field appeared to radiate outward, and the vertical displacement exceeded the horizontal displacement. Whether this result is an artifact or a consequence of mass movement cannot be determined from the data; therefore, it should be interpreted with caution.

[29] The temporal evolution of the pixel offsets explosion is non-reversible, as illustrated in Figure 6a, which shows the mean displacement of region RE1 relative to the first image. Figure 6b shows the total displacement before and after the explosion. If the displacements associated with the explosions are separated into horizontal (Vx) and vertical (Vy) components (Figure 6a), the Vx component displays a pronounced step-like movement to the right of the field of view. In contrast, the Vy component reveals a decaying displacement value with a negative sign. The proportion of the stepwise Vy displacement that is directly associated with the explosion is followed by almost the same proportion of post-explosive displacement. Therefore, horizontal and outward movements are instantaneous, whereas the downward movement appears to be a more sustained process that can last up to ~10 min.

[30] The single explosion example demonstrates the utility of infrared DIC. The results of a complete time series of a night recording are provided in Figure 7. For comparison and validation, we used the positive mean temperature change above the dome (region RE2; Figure 7a). Although images taken during the first few hours of the night (up to 19:00 local time) were affected by cloud cover (see also supporting information SI), subsequent data showed six pronounced exhalation spikes. Such pronounced image temperature spikes were previously recorded and interpreted to be due to a Vulcanian-style eruption [*Stevenson and Varley*, 2008].

[31] Dome-deformation data obtained from the DIC are shown in Figure 7b. The pixel offset is determined from a five-frame interval. Consequently, the velocity scale of the pixels located in region RE1 can be calculated. The first two explosion events are relatively small and reach up to 10 cm. The last three displacements occur over longer periods (8, 13, and 14 min) and reach up to 20, 35, and 28 cm within 5 frames respectively. We observed a temporal relationship between these stepwise growths and the seismic amplitude release (Figure 7). The seismic data are shown at a sampling frequency approximately 2 orders of magnitude higher than the time-lapse frequency. We plotted the RSAM to show the timing of the main periods of unrest. We found that all of the RSAM peaks occur concomitantly with dome-deformation episodes.

[32] Of the six identified thermal exhalation events, only five exhibited stepwise and very pronounced displacement changes (labeled 1 to 5 in Figure 7). However, only four of these can be observed in the RSAM plot (labeled 1, 3, 4, and 5 in Figure 7). Therefore, our data imply that in some cases, (i) thermal exhalations may occur without deformation or seismicity detection and (ii) significant displacement peaks exist but are not always associated with detectable seismic amplitude increases. In particular, for approximately 8 h of the night recording, no RSAM peaks were detected in the 1 s RSAM plots, although the camera records clearly indicate the occurrence of an explosion at 23:14 (local time), as demonstrated by both the thermal exhalation and an approximately 8 cm mean displacement rate of the dome in 5

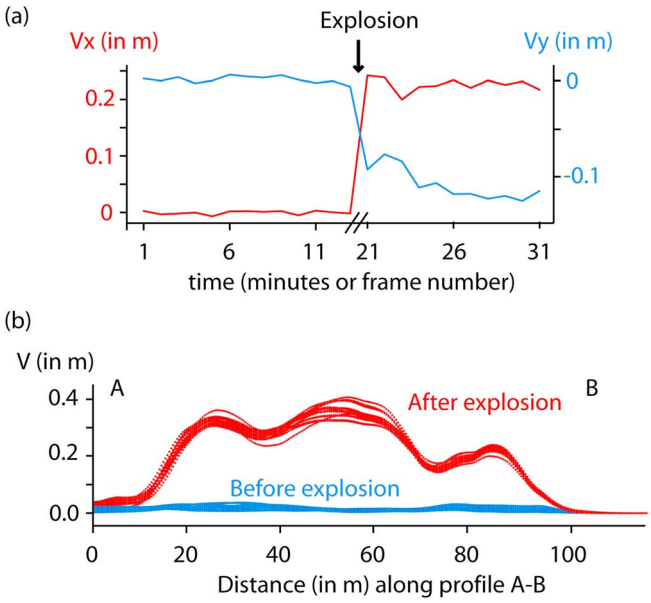

Figure 6. (a) Comparison of the mean horizontal (Vx) and vertical (Vy) displacements calculated for region RE1 (see Figure 4 for the location). The first image is the reference image, with which each subsequent image is cross-correlated. For visualization purposes, we show every fifth image only. Note the occurrence of a generally stepwise deformation without precursory deformation. Vx ends after the explosion, whereas Vy continues for up to ~10 min. (b) Displacement occurred along profile A-B, as indicated in frame 6 of Figure 4a. The largest displacement occurred at the center and above.

minutes. This result may be explained by a number of factors, such as the difference in the sensitivities of the camera and the seismograms or the occurrence of seismically silent (aseismic) deformation events. A 1 min RSAM plot and the direct observations from the seismograms support the occurrence of a missing event at 23:14 (see supporting information), although the event was classified as a rock fall and not an eruption event.

4. Discussion

[33] This study utilized infrared time-lapse imagery to detect and quantify volcanic dome-deformation episodes. Using thermal camera data, we closely observed temporal and spatial variations in the dome and temperature distribution. Using a modern image-correlation method, we traced the thermal field across multiple images, which allowed us to identify thermal exhalations and episodes of pixel offsets and, consequently, to quantify the associated deformation and directivity of displacement.

4.1. DIC Volcano Deformation Monitoring: Limitations and Advantages

[34] The monitoring of the deformation of dome volcanoes is often limited by their steep topography, rock falls, and avalanches as well as other issues pertaining to instrumentation and data quality. Therefore, volcano deformation monitoring relies on (a) in situ instrumentation located in the middle and lower flanks of volcanoes, such as instruments that measure position, tilt, or a triangulate network; (b) satellite radar studies using InSAR, which provide information at high spatial but low temporal resolution; and, in many cases, (c)

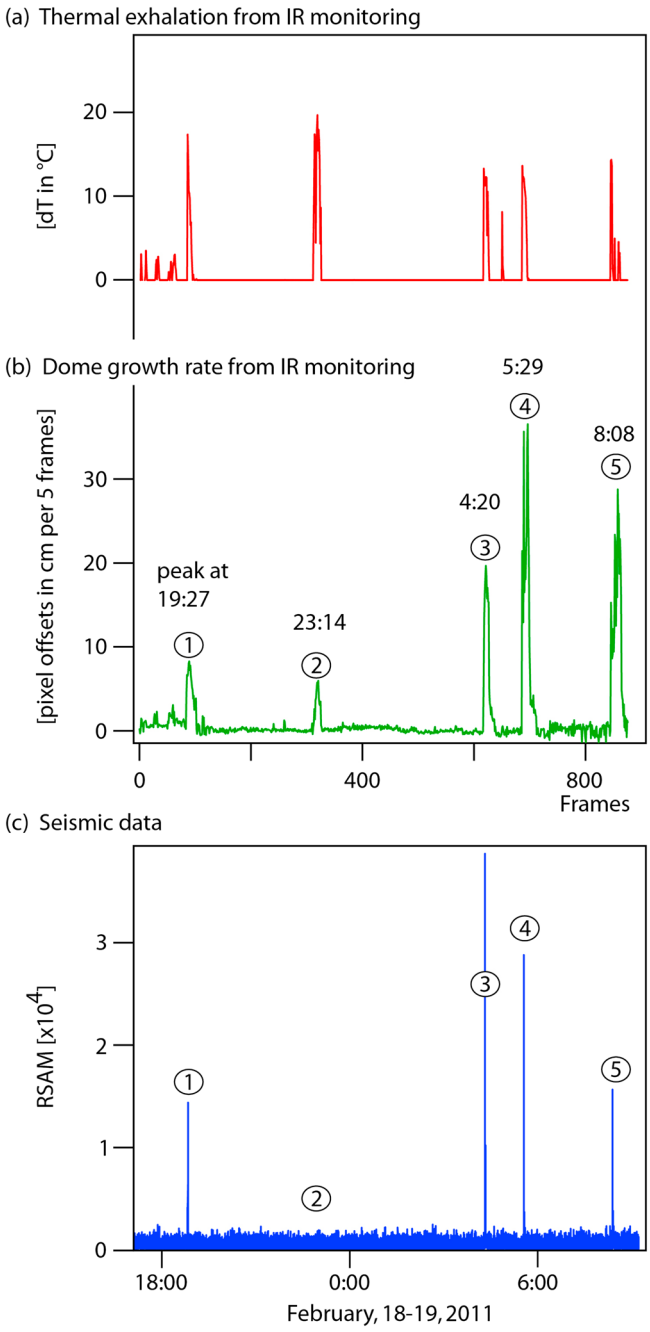

Figure 7. Comparison of (a) thermal exhalation (in red, extracted from RE1 in Figure 4) and (b) deformation data (in green, extracted from RE2 in Figure 4) against (c) seismic amplitude data (in blue) for a 15 h time series. In total, five main displacement peaks (labeled as dome growth) occurred, with peaks at 19:27, 23:14, 4:20, 5:29 and 8:08 (local times). All of these dome-growth episodes were associated with thermal exhalations. Note the ~8 h calm RSAM period that occurred near midnight, although the camera records indicate that displacements and thermal exhalation occurred during this time.

observations with the human eye. None of these approaches were conducive to enabling the direct monitoring of the dome growth of Volcán de Colima or of most other similarly steep-sided and rapidly changing volcanoes.

[35] Imaging methods have been applied for decades to study volcanic processes [*Francis and Rothery*, 2000]. Focusing on satellite-based methods for many years, the study of active and passive remote-sensing systems has enabled the analysis of changes in volcano activity worldwide. When applied to dome-building volcanoes, however, the sparse temporal and spatial resolution of satellite-based methods is commonly limiting. Landsat imagery, for instance, with its resolution of >200 m^2 and revisit times of 16–18 days, allows for the detection of first-order temporal and spatial changes only [*Flynn et al*., 2001]. Although more modern satellite sensors may significantly contribute to volcano activity assessment [*Flynn et al*., 2001; *Pallister et al*., 2012], environmental artifacts and poor temporal and spatial resolution may limit the application of many sensors at rapidly deforming and dome-building volcanoes [*Coppola et al*., 2010; *Pinel et al*., 2011].

[36] The benefits of "handheld" video and camera monitoring methods are related to the technically immense spatiotemporal resolution and flexible application possibilities. Images taken from a helicopter allow almost any viewing geometry to be combined into digital elevation models using photogrammetry and other computer vision methods [*Diefenbach et al*., 2012; *James and Varley*, 2012]. Ground-based video and camera monitoring methods from stable positions are increasingly used to continuously observe active dome-building volcanoes and their morphological changes, luminance, and eruption occurrence, such as at Mount St. Helens in the U.S. [*Major et al*., 2008; *Major et al*., 2009], Merapi in Indonesia [*Ratdomopurbo*, 1995], and Mount Unzen in Japan [*Kaneko et al*., 2002].

[37] Pixel offset determinations have been carried out on satellite optical data [*Gonzalez et al*., 2010], satellite radar data [*Jonsson et al*., 2005], aerial photography [*Tseng et al*., 2009], ground-based optical data [*James et al*., 2012], ground-based infrared data (this work), and (rock) experimental tests [*White et al*., 2003]. As demonstrated in the present work, the determination of pixel offsets using the DIC method is especially useful for volcanic domes that are subject to deformation and collapse as well as those that experience episodic explosions. As shown earlier for the Santiaguito volcano, pixel-offset calculations are particularly useful when conventional geodetic techniques are difficult or too dangerous to use [*Johnson et al*., 2008]. By applying this technique to infrared imaging, we highlight the advantage of its use at night, a time when there is less atmospheric and solar disturbance and when most other video monitoring methods do not provide much information. Another major advantage is that the relationship between the location of events on an active dome and the occurrence of the thermal exhalations can be directly investigated.

[38] Our results are based on ~900 infrared images, corresponding to one full night of recording during one of the most active periods of dome growth at Volcán de Colima. The fastest deformation episode determined in the RE1 subregion exceeded ~0.3 m of lateral displacement of the dome flanks within 5 min. Our results show that not all of these dome-growth episodes were associated with seismic amplitude peaks but all of these episodes were associated with detectable thermal exhalations. The results also show that the dome-deformation episodes are non-reversible; thus, they may potentially differ from earlier observations [*Johnson et al*., 2008].

[39] The detection threshold of techniques relying on particle image velocimetry or digital image correlation (the former is traditionally developed for and applied to fluid dynamic observations, whereas the latter is applied to solid body deformations) is thought to be close to 1/10 of a pixel dimension in natural environments. As our own tests from the stable parts of the Colima dome show, the level of background noise in small interrogation windows is on the order of ~5 cm. Computation of the mean displacement increases the signal-to-noise ratio and accordingly reduces the noise level to ~2 cm. Although a quantitative assessment of the accuracy of the technique is site dependent and would ideally require independent in situ geodetic observations, a comparison with seismic data at the Volcán de Colima suggests that the detection threshold is sufficiently low to enable the measurement of all significant episodes of dome deformation.

4.2. Are the Eruptions of Vulcanian Style?

[40] For the Volcán de Colima, pronounced image temperature maxima have been previously interpreted to represent Vulcanian eruption styles i.e., low amounts of or no juvenile magma escaping from the vent. Similar to the findings of *Stevenson and Varley* [2008], we found that the occurrence of explosions, as detected by thermal exhalations, was well represented in the imagery data. Furthermore, our image-correlation analysis demonstrated that these thermal exhalations are in fact temporally associated with the dome-deformation episodes. Assuming that the deformation is indeed related to dome growth, the eruptions of Volcán de Colima may contain significant amounts of fresh magmatic material. For gas to extrude from the dome, the gas content, as evidenced by the thermal exhalations, may be a determining parameter because the pressure release associated with an ascending magma body can lead to gas exsolution and expansion [*Jaupart and Allègre*, 1991; *Johnson et al*., 2008]. According to *Jaupart and Allègre* [1991], the dome extrusion rate is inversely proportional to the amount of gas lost and proportional to the pressure difference between the conduit and the volcanic rock. Our data, however, do not reveal a scale dependency of the deformation and exhalation events; that is, we could not find any meaningful correlation between large exhalations and the associated displacements. This finding may mean that the deformations observed at the western part of the Colima dome, possibly representing a coulée-like flow, are not directly scaled to dome-growth episodes. Also, it may mean that the thermal exhalation data is not allowing quantitative interpretation, as infrared signals may be damped by gas and water vapor.

4.3. Aseismic Dome Deformation

[41] The reason the lateral displacement of a dome (on the order of 20 to 30 cm within a few minutes) is not always observable in the seismic recordings remains a mystery and may result from incorrect data recording or analysis. Assuming that the closest available broadband seismic stations are adequately sensitive, averaging the data over 1 min or more may lead to less noisy plots and, therefore, slightly different results (see the supporting information). Both types of

explosions, those that are accompanied by seismic signals and those that are not, were identified in the camera data, as illustrated in the full video sequence accompanying this paper. Errors arising from overall image shifts or other issues were ruled out by validation of the stability of pixels far from the deformed dome.

[42] Our analysis of the seismic data and the pixel offsets calculated from the images, together with the identification of exhalation above the dome, suggests that (1) the independent data are well validated, but (2) the camera data can detect events that are not accompanied by detectable seismic signals. One explanation for this result is that some of the dome-growth episodes occur without the release of much seismic and/or explosive energy. Assuming that the interface between the dome and the host rock resembles a shear plane (a fault), similarities to other faults that slip aseismically may be considered [*Brooks et al*., 2008]. Similarly, it can be hypothesized that the deforming sectors of a silicic dome may be displaced without significant seismic energy release. In this respect, it remains unclear whether the degassing events (exhalations) are causing or facilitating the displacement of the dome or are a consequence thereof [*Jaupart and Allègre*, 1991; *Johnson et al*., 2008]. However, continuous dome growth and the extrusion of different rock types, such as an impermeable plug, have important consequences for the stability of the edifice [*Lavallee et al*., 2012] and may therefore alter the success of the seismic and deformation detection methods.

4.4. Modality of Dome Growth and Further Implications

[43] The dome of the Volcán de Colima, which grew almost continuously between 2007 and 2011, was found to have mostly cooled down; growth that occurred during February 2011 was directed mainly toward the west. As the amount of displacement is larger at the uppermost part of hot dome, it may be speculated that forceful extrusion pushes lateral slices of thermally elevated regions. Although the temporal resolution of the infrared camera was poor, when accompanied by seismicity, RSAM peaks were found to occur just at the beginning or slightly before extrusion events (Figure 7c). As the initial deformation is mainly horizontal, followed by a predominantly vertical deformation of the western dome in subsequent minutes, we interpret the deformation to be driven by a combination of active extrusion and gravity-driven sagging (Figure 8). Adapting the concept of *Lavallee et al*. [2012] that a solid plug underneath the older parts of a dome may divert the magma path, we conjecture that the magma conduit under Volcán de Colima is asymmetric. The conduit is currently focused on the west side, causing extrusion and deformation of the dome toward the west (Figure 8). Moreover, the preexisting topography and absence of a buttress on the west side further favors the growth and displacement of the western dome.

4.5. Further Limitations and Implications

[44] This study did not attempt to investigate the absolute temperatures of the volcano because no in situ temperature comparison or robust atmospheric correction was performed. The absolute field was irrelevant for the application of the digital image correlation term, which relied on normalized values. However, a variety of other factors may have affected the

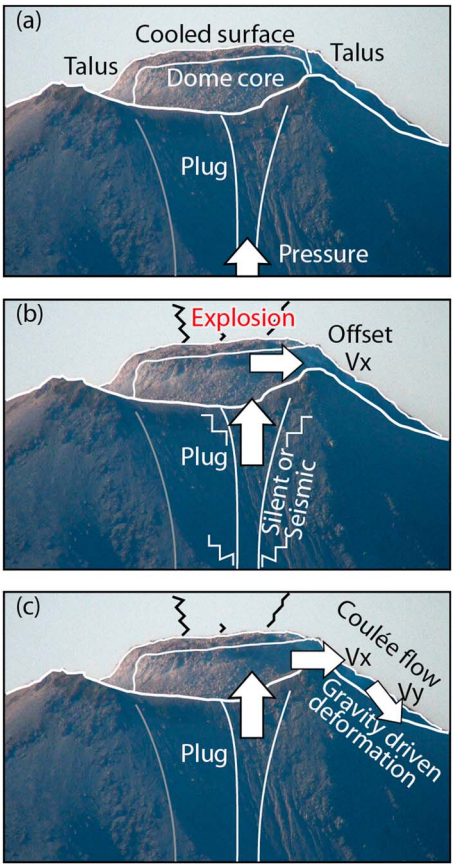

Figure 8. Conceptual model of (a) seismicity occurrence during dome extrusion, (b) thermal exhalation during explosion and lateral deformation (Vx) of the hot part of the dome, and (c) relative increase in the gravity-driven deformation component (Vy) of the dome. Shear exists at the Colima conduit wall and was likely localized on one side only, as a plug may be diverting the magma ascent path.

results. One has to consider the effect of a gassy atmosphere, especially during the exhalation events [*Sawyer and Burton*, 2006]. As detailed above, the travel path of the signal may be affected by any particles and by gas, biasing the derived temperature values. The brightness temperature of an affected pixel may change, resulting in pixel translation artifacts. However, in the data presented, we could not determine a systematic agreement between the sites of pixel shifts (occurring on the west flank of the dome) and the thermal exhalation sites (occurring on the summit of the dome).

[45] We interpreted determined pixel offsets to be related to deformation. Possibly, the thermal pattern, rather than the rock mass, is laterally migrating. Given that an eruption event at Colima volcano is associated with a significant and detectable lateral systematic shift in the fumarole locations (while the rock mass is stable), our interpretation of a deformation occurrence would not hold. However, although infrared surveys elsewhere describe a lateral migration of fumaroles [*Matsushima et al*., 2003], a very systematic and directed shift that is also nonreversible and cumulative appears unlikely. Although this cannot be ruled out, we assume that our interpretation of a rigid body movement is valid and physically more sound.

[46] Sub-pixel variabilities, such as a change in the surface characteristics and temperature pattern, may affect the results of any imaging technique. In our case, assuming that a fumarole with a typical dimension of 10^{-1} m^2 is detected and several such fumaroles are present in one pixel, a temperature change in one or more of these fumaroles may be reflected as a total brightness change of the pixel and be interpreted as a sub-pixel shift. Therefore, sub-pixel variabilities may act as a source of error and require more rigorous quantification in future work.

[47] Despite these limitations, the method applied here to monitor the growth activity of the Colima dome is very promising and may even allow for the quantification of the size of extrusions and explosions. As we have demonstrated in this study, the amount of dome deformation is not directly (linearly) related to the size of the RSAM. As the RSAM is the sum of all types of seismic activity, it does not provide enough information to determine the size of an eruption. Instead, camera observations may provide the necessary data streams to quantify the displacements and the material fluxes, especially if several cameras are combined.

5. Conclusions

[48] An infrared digital image correlation analysis of data recorded at the Volcán de Colima dome during February 2011 was performed to monitor the occurrence of thermal explosions and their association with deformation events (in terms of infrared pixel offsets) and real-time seismic amplitude measurements (RSAM). Of the six thermal exhalations that were likely associated with the explosions, deformation was detected in association with five. Of these five deformation events, only four were associated with seismically detected activity. The data imply that all of the detected events were accompanied by thermal changes. However, some significant deformations may occur without the accompaniment of any seismicity, which may reflect silent or slow deformation processes that occur in dome-building volcanoes.

[49] **Acknowledgments.** We thank Bo Galle for suggesting Colima as a camera-testing site and for the invitation to conduct joint fieldwork. We acknowledge financial support from the Helmholtz Fund "Initiating and Networking," the HGF Aliance "Remote Sensing and Earth System Dynamics," the GFZ Potsdam grant, and the FONCICyT-93645 grant. The work was improved by thorough and constructive reviews by Mike James and Letizia Spampinato.

References

Anonymous (2003), Hobrough, Gilbert Louis, *Photogramm. rec.*, *18*(104), 337–340.

Ball, M., and H. Pinkerton (2006), Factors affecting the accuracy of thermal imaging cameras in volcanology, *J. Geophys. Res-Solid Earth*, *111*(B11).

Belousov, A., M. Belousova, and B. Voight (1999), Multiple edifice failures, debris avalanches and associated eruptions in the Holocene history of Shiveluch volcano, Kamchatka, Russia, *Bull. Volcanol.*, *61*(5), 324–342.

Brooks, B. A., J. Foster, D. Sandwell, C. J. Wolfe, P. Okubo, M. Poland, and D. Myer (2008), Magmatically triggered slow slip at Kilauea Volcano, Hawaii, *Science*, *321*(5893), 1177.

Christiansen, R. L., and D. W. Peterson (1981), The 1980 eruptions of Mount St. Helens, Washington. Chronology of the 1980 eruptive activity, *U.S. Geol. Surv. Prof. Pap.*, *1250*, 17–30.

Clocksin, W. F., J. Quinta da Fonseca, P. J. Withers, and P. H. S. Torr (2002), Image processing issues in digital strain mapping, *Proc. SPIE*, *4790*, 384–395.

Coppola, D., M. R. James, T. Staudacher, and C. Cigolini (2010), A comparison of field- and satellite-derived thermal flux at Piton de la Fournaise: Implications for the calculation of lava discharge rate, *Bull. Volcanol.*, *72*(3), 341–356.

Davila, N., L. Capra, J. C. Gavilanes-Ruiz, N. Varley, G. Norini, and A. G. Vazquez (2007), Recent lahars at Volcan de Colima (Mexico): Drainage variation and spectral classification, *J. Volcanol. Geotherm. Res.*, *165*(3-4), 127–141.

Diefenbach, A. K., J. G. Crider, S. P. Schilling, and D. Dzurisin (2012), Rapid, low-cost photogrammetry to monitor volcanic eruptions: An example from Mount St. Helens, Washington, USA, *Bull. Volcanol.*, *74*(2), 579–587.

Donnadieu, F. (2000), Destabilisation des edifices volcaniques par les cryptodomes: Modelisation analogique et approche numerique. Volcanic edifice destabilization through cryptodome emplacement: Analog modelling and numerical approach, Ecole Doctorale des Sciences Fondamentales, vol. 267, 256 pp, Universite Blaise Pascal, Clermont-Ferrand II, Clermont-Ferrand, France (FRA).

Dzurisin, D. (2007), Volcano Deformation: Geodetic Monitoring Techniques, 441 pp, Praxis Publishing, Chichester, United Kingdom.

Endo, E. T., and T. Murray (1991), Real-time seismic amplitude measurement (RSAM): A volcano monitoring and prediction tool, *J. Volcanol. Geotherm. Res.*, *57*(7), 533–545.

Fink, J. H., and S. W. Anderson (2000), *Lava Domes and Coulees*, pp. 307–319, Academic Press, San Diego, Calif.

Flynn, L. P., A. J. L. Harris, and R. Wright (2001), Improved identification of volcanic features using Landsat 7 ETM+, *Remote Sens. Environ.*, *78*(1–2), 180–193.

Formenti, Y., T. H. Druitt, and K. Kelfoun (2003), Characterisation of the 1997 Vulcanian explosions of Soufriere Hills Volcano, Montserrat, by video analysis, *Bull. Volcanol.*, *65*(8), 587–605.

Francis, P., and D. Rothery (2000), Remote sensing of active volcanoes, *Annu. Rev. Earth Planet. Sci.*, *28*, 81–106.

Gonzalez, P. J., M. Chini, S. Stramondo, and J. Fernandez (2010), Coseismic horizontal offsets and fault-trace mapping using phase correlation of IRS satellite images: The 1999 Izmit (Turkey) earthquake, *Ieee Trans. Geosci. Remote Sens.*, *48*(5), 2242–2250.

Hooper, D. M., and G. S. Mattioli (2001), Kinematic modeling of pyroclastic flows produced by gravitational dome collapse at Soufriere Hills volcano, Monstserrat, *Nat. Hazard.*, *23*(1), 65–86.

Hort, M., M. Voge, R. Seyfried, and A. Ratdomopurbo (2006), In situ observation of dome instabilities at Merapi volcano, Indonesia: A new tool for volcanic hazard mitigation, *J. Volcanol. Geotherm. Res.*, *153*(3-4), 301–312.

James, M. R., and N. Varley (2012), Identification of structural controls in an active lava dome with high resolution DEMs: Volcán de Colima, Mexico, *Geophys. Res. Lett.*, *39*(22), L22303.

James, M. R., H. Pinkerton, and S. Robson (2007), Image-based measurement of flux variation in distal regions of active lava flows, *Geochem. Geophys. Geosyst.*, *8*, Q03006.

James, M. R., H. Pinkerton, and L. J.. Applegarth (2009), Detecting the development of active lava flow fields with a very-long-range terrestrial laser scanner and thermal imagery, *Geophys. Res. Lett.*, *36*.

James, M. R., L. J. Applegarth, and H. Pinkerton (2012), Lava channel roofing, overflows, breaches and switching: insights from the 2008-9 eruption of Mt. Etna, *Bull. Volcanol.*, *74*(1), 107–117.

Jaupart, C., and C. J. Allègre (1991), Gas content, eruption rate and instabilities of eruption regime in silicic volcanoes, *Earth Planet. Sci. Lett.*, *102*, 413–429.

Jimenez-Escalona, J., H. Granados, and V. Realmuto (2011), Use of MODIS images to study eruptive clouds from Volcan de Fuego de Colima (Mexico) and applications on volcano monitoring, *Geofis. Int.*, *50*(2), 199–210.

Johnson, J. B., J. M. Lees, A. Gerst, D. Sahagian, and N. Varley (2008), Long-period earthquakes and co-eruptive dome inflation seen with particle image velocimetry, *Nat. (London)*, *456*(7220), 377–381.

Jonsson, S., H. Zebker, and F. Amelung (2005), On trapdoor faulting at Sierra Negra volcano, Galapagos, *J. Volcanol. Geotherm. Res.*, *144*(1-4), 59–71.

Kaneko, T., M. J. Wooster, and S. Nakada (2002), Exogenous and endogenous growth of the Unzen lava dome examined by satellite infrared image analysis, *J. Volcanol. Geotherm. Res.*, *116*(1-2), 151–160.

Konecny, G. (1985), The international society for photogrammetry and remote sensing—75 years old, or 75 years young, *Photogramm. Eng. Remote Sens.*, *51*(7), 919–933.

Lavallee, Y., N. R. Varley, M. A. Alatorre-Ibarguengoitia, K. U. Hess, U. Kueppers, S. Mueller, D. Richard, B. Scheu, O. Spieler, and D. B. Dingwell (2012), Magmatic architecture of dome-building eruptions at Volcan de Colima, Mexico, *Bull. Volcanol.*, *74*(1), 249–260.

Luhr, J. F. (2002), Petrology and geochemistry of the 1991 and 1998–1999 lava flows from Volcan de Colima, Mexico; implications for

the end of the current eruptive cycle, *J. Volcanol. Geotherm. Res.*, *117* (1-2), 169–194.

Luhr, J. F., and I. S. E. Carmichael (1980), The Colima volcanic complex, Mexico. I, Post-caldera andesites from Volcan Colima, *Contrib. Mineral. Petrol.*, *71*(4), 343–372.

Luhr, J. F., P. Kimberly, L. Siebert, J. J. Aranda-Gomez, T. B. Housh, and G. K. Mattietti (2006), Mexico's Quaternary volcanic rocks: Insights from the MEXPET petrological and geochemical database, *Spec. Pap. - Geol. Soc. Am.*, *402*, 1–44.

Major, J. J., C. G. Kingsbury, M. P. Poland, and R. G. LaHusen (2008), Extrusion rate of the Mount St. Helens lava dome estimated from terrestrial imagery, November 2004–December 2005, *U. S. Geological Survey Professional Paper*, *1750*, 237–255.

Major, J. J., D. Dzurisin, S. P. Schilling, and M. P. Poland (2009), Monitoring lava-dome growth during the 2004–2008 Mount St. Helens, Washington, eruption using oblique terrestrial photography, *Earth Planet. Sci. Lett.*, *286*(1-2), 243–254.

Matsushima, N., K. Kazahaya, G. Saito, and H. Shinohara (2003), Mass and heat flux of volcanic gas discharging from the summit crater of Iwodake volcano, Satsuma-Iwojima, Japan, during 1996–1999, *J. Volcanol. Geotherm. Res.*, *126*(3-4), 285–301.

Mendoza-Rosas, A. T., and S. de la Cruz-Reyna (2008), A statistical method linking geological and historical eruption time series for volcanic hazard estimations: Applications to active polygenetic volcanoes, *J. Volcanol. Geotherm. Res.*, *176*(2), 277–290.

Orr, T. R., and J. C. Rea (2012), Time-lapse camera observations of gas piston activity at Pu'u 'Ō'ō, Kīlauea volcano, Hawai`i, *Bull. Volcanol.*, *75*(10), 2353–2362.

Pallister, J. S., D. J. Schneider, J. P. Griswold, R. H. Keeler, W. C. Burton, C. Noyles, C. G. Newhall, and A. Ratdomopurbo (2012), Merapi 2010 eruption—Chronology and extrusion rates monitored with satellite radar and used in eruption forecasting, *J. Volcanol. Geotherm. Res.*, *Available online 1 August 2012*.

Pan, B., K. Qian, H. Xie, and A. Asundi (2009), Two-dimensional digital image correlation for in-plane displacement and strain measurement: A review, *Meas. Sci. Technol.*, *20*(062001), 1–17.

Patrick, M. R., J. P. Kauahikaua, and L. Antolik (2010), MATLAB tools for improved characterization and quantification of volcanic incandescence in Webcam imagery: Applications at Kilauea Volcano, Hawai`i, *U.S. Geol. Surv. Tech. Methods*, *13*(A1), 1–16.

Peters, W. H., and W. F. Ranson (1982), Digital imaging techniques in experimental stress analysis, *Opt. Eng.*, *21*(3), 427–431.

Peters, W. H., Z.-H. He, M. A. Sutton, and W. F. Ranson (1984), Two-dimensional fluid velocity measurements by use of digital speckle correlation techniques, *Exp. Mech.*, *24*(2), 171–121.

Petersen, G. N., H. Bjornsson, and P. Arason (2011), The impact of the atmosphere on the Eyjafjallajökull 2010 eruption plume, *J. Geophys. Res.*, *117*(D00U07), 1–14.

Pinel, V., A. Hooper, S. de la Cruz-Reyna, G. Reyes-Davila, M. P. Doin, and P. Bascou (2011), The challenging retrieval of the displacement field from InSAR data for andesitic stratovolcanoes: Case study of Popocatepetl and Colima Volcano, Mexico, *J. Volcanol. Geotherm. Res.*, *200*(1-2), 49–61.

Ramirez-Ruiz, J. J., H. Santiago-Jimenez, E. Alatorre-Chavez, and M. Breton-Gonzalez (2002), EDM deformation monitoring of the 1997–2000 activity at Volcan de Colima, *J. Volcanol. Geotherm. Res.*, *117*(1–2), 61–67.

Ramsey, M. S., and A. J. L. Harris (2012), Volcanology 2020: How will thermal remote sensing of volcanic surface activity evolve over the next decade?, *J. Volcanol. Geotherm. Res.*, *in press*.

Ratdomopurbo, A. (1995), Etude sismologique du volcan Mérapi et formation du dôme de 1994, 208 pp, University of Joseph Fourier, Grenoble.

Saucedo, R., J. L. Macias, J. C. Gavilanes, J. L. Arce, J. C. Komorowski, J. E. Gardner, and G. Valdez-Moreno (2010), Eyewitness, stratigraphy, chemistry, and eruptive dynamics of the 1913 plinian eruption of Volcan de Colima, Mexico, *J. Volcanol. Geotherm. Res.*, *191*(3–4), 149–166.

Sawyer, G. M., and M. R. Burton (2006), Effects of a volcanic plume on thermal imaging data, *Geophys. Res. Lett.*, *33*(14).

Schneider, D. J., J. W. Vallance, R. L. Wessels, M. Logan, and M. S. Ramsey (2008), Use of thermal infrared imaging for monitoring renewed dome growth at Mount St. Helens, 2004, *U. S. Geol. Surv. Prof. Pap.*, *1750*, 347–359.

Schreier, H. W., J. R. Braasch, and M. A. Sutton (2000), On systematic errors in digital image correlation, *Opt. Eng.*, *39*(11), 2915–2921.

Spampinato, L., S. Calvari, C. Oppenheimer, and E. Boschi (2011), Volcano surveillance using infrared cameras, *Earth-Sci. Rev.*, *106*(1–2), 63–91.

Stevenson, J. A., and N. Varley (2008), Fumarole monitoring with a handheld infrared camera; Volcan de Colima, Mexico, 2006–2007, *J. Volcanol. Geotherm. Res.*, *177*(4), 911–924.

Sutton, M., W. J. Wolters, W. H. Peters, W. F. Ranson, and S. R. McNeill (1983), Determination of displacements using an improved digital correlation method, *Image Vision Comput.*, *1*(3), 133–139.

Sutton, M. A., J.-J. Orteu, and H. Schreier (2009), *Image Correlation for Shape, Motion and Deformation Measurements: Basic Concepts,Theory and Applications*, 342 pp., Springer, New York.

Tseng, C.-H., J.-C. Hu, Y.-C. Chan, H.-T. Chu, J.-F. Lee, J.-Y. Wei, C.-Y. Lu, and M.-L. Lin (2009), Non-catastrophic landslides induced by the Mw 7.6 Chi-chi earthquake in central Taiwan as revealed by PIV analysis, *Tectonophysics*, *466*(3-4), 427–437.

Voight, B. (2000), Structural stability of andesite volcanoes and lava domes, *Philos. Trans. R. Soc. London*, *358*(1770), 1663–1703.

Voight, B., and D. Elsworth (2000), Instability and collapse of hazardous gas-pressurized lava domes, *Geophys. Res. Lett.*, *27*(1), 1–4.

Walter, T. R. (2011a), Low cost volcano deformation monitoring: Optical strain measurements and application to Mount St. Helens data, *Geophys. J. Int.*, *186*(2), 699–705.

Walter, T. R. (2011b), Structural architecture of the 1980 Mount St. Helens collapse: an analysis of the Rosenquist photo sequence using digital image correlation, *Geology (Boulder)*, *39*(8), 767–770.

White, D. J., W. A. Take, and M. D. Bolton (2003), Soil deformation measurement using particle image velocimetry (PIV) and photogrammetry, *Geotech.*, *53*(7), 619–631.

Yamashina, K., T. Matsushima, and S. Ohmi (1999), Volcanic deformation at Unzen, Japan, visualized by a time-differential stereoscopy, *J. Volcanol. Geotherm. Res.*, *89*, 73–80.